remote sensing

MDPI

Technical Note

Impact of Urbanization on Cloud Characteristics over Sofia, Bulgaria †

Ventsislav Danchovski

Department of Meteorology and Geophysics, Faculty of Physics, Sofia University, 1164 Sofia, Bulgaria; danchovski@phys.uni-sofia.bg

† This paper is an extended version of the conference proceedings contribution "Urban effects on cloud base height and cloud persistence over Sofia, Bulgaria" presented at the International Electronic Conference on Remote Sensing, 7–21 November 2023.

Abstract: Urban artificial surfaces and structures induce modifications in land–atmosphere interactions, affecting the exchange of energy, momentum, and substances. These modifications stimulate urban climate formation by altering the values and dynamics of atmospheric parameters, including cloud-related features. This study evaluates the presence and quantifies the extent of such changes over Sofia, Bulgaria. The findings reveal that estimations of low-level cloud base height (CBH) derived from lifting condensation level (LCL) calculations may produce unexpected outcomes due to microclimate influence. Ceilometer data indicate that the CBH of low-level clouds over urban areas exceeds that of surrounding regions by approximately 200 m during warm months and afternoon hours. Moreover, urban clouds exhibit reduced persistence relative to rural counterparts, particularly pronounced in May, June, and July afternoons. Reanalysis-derived low-level cloud cover (LCC) shows no significant disparities between urban and rural areas, although increased LCC is observed above the western and northern city boundaries. Satellite-derived cloud products reveal that the optically thinnest low-level clouds over urban areas exhibit slightly higher cloud tops, but the optically thickest clouds are more prevalent during warm months. These findings suggest an influence of urbanization on cloudiness, albeit nuanced and potentially influenced by the city size and surrounding physical and geographical features.

Keywords: urban climate; cloud base height; cloud persistence; urban heat island

Citation: Danchovski, V. Impact of Urbanization on Cloud Characteristics over Sofia, Bulgaria. *Remote Sens.* **2024**, *16*, 1631. https://doi.org/10.3390/rs16091631

Academic Editor: Alexander Kokhanovsky

Received: 4 March 2024
Revised: 28 April 2024
Accepted: 29 April 2024
Published: 2 May 2024

1. Introduction

Clouds play a fundamental role in Earth's climate dynamics by controlling incoming radiation through alterations in atmospheric transparency and planetary albedo [1]. Additionally, cloud cover influences the longwave radiation emitted by the surface [2] and thus governs the Earth's energy budget [3]. Given their pivotal role in the water cycle, clouds facilitate the transport of latent heat and water vapor [4]. Notably, clouds above urban areas control the shortwave energy available for absorption by solar panels, thus influencing the feasibility of transitioning to sustainable energy sources [5]. Furthermore, the risk and hazard of certain natural disasters is also associated with clouds and storms [6].

Cloud formation is a result of natural processes that span different scales, from micro (condensation) to synoptic (cyclones) and even planetary ones (the Intertropical Convergence Zone) [7]. It appears that urban impacts on clouds and precipitation may also occur [8–11]. Cloud base height (CBH) has been found to be higher over cities, which is attributed to the presence of warmer, drier, and stronger updrafts emanating from urbanized regions compared to their rural counterparts [12]. Moreover, alterations in cloud cover have been documented over urban areas [13]. The observed urban influence on cloud dynamics and precipitation regimes has been proposed to stem from enhanced turbulent mixing and thermally driven convection associated with the urban heat island-induced

circulation [14–16]. Furthermore, increased roughness over urban areas induces surface convergence, leading to forced updrafts on the windward side and downdrafts on the leeward side, although the direct effects of roughness can sometimes be minimal [17,18]. Disparities in surface characteristics between urban and rural landscapes give rise to the formation of an urban boundary layer that can be cloud-covered [19]. Furthermore, hygroscopic pollutants emitted into the urban atmosphere can act as cloud condensation nuclei, thereby altering cloud microphysics [20–24]. However, urban land cover and emitted aerosols may have an opposite effects, often resulting in reduced precipitation over urban areas and enhanced precipitation downwind [25]. Favorable conditions for urban modification, typically observed during late afternoon summer periods with weak synoptic forcing, have been linked to increased thunderstorm frequency and intensity downwind of large cities; however, under nonoptimal conditions, upwind areas may experience intensified thunderstorms relative to downwind regions [26]. Additionally, some authors found that urban areas may serve as barriers, leading to the bifurcation of summer thunderstorms and resulting in reduced rainfall directly over urban centers [27].

Detecting and quantifying the urban impact on clouds in a continuously moving atmosphere poses significant challenges, as clouds formed over the rural area might be advected towards the urban area by the prevailing winds [28]. Moreover, many cities are settled close to the borders of natural landscapes with contrasting physical properties (e.g., sea–land, mountain–valley), and this modifies background atmospheric flows and produces local ones that can cause changes in the clouds, which are difficult to isolate and exclude [29]. Identifying urban influence requires precise quantification of the cloud features with high temporal resolution, reducing the reliability of human-made cloud observations [30]. Measurements of near-surface air humidity, temperature, and atmospheric pressure allows for estimation of the lifting condensation level (LCL), representing the altitude at which adiabatically lifted air parcels become saturated and cloud formation is initiated [31]. Although the LCL serves as a proxy for cloud base height, its suitability for non-convective clouds is uncertain. Alternatively, analysis of relative humidity profiles collected during rawinsonde flights enables the inference of cloud presence and estimation of cloud base height [32]. Ceilometers, widely used as reference instruments for cloud base height determination, employ laser-based lidar technology to measure the round-trip time of laser pulses emitted towards clouds [33–35]. While traditionally used for air traffic safety at airports and atmospheric reanalysis validation [36], ceilometers have obtained increased attention for diverse applications within pan-European initiatives [37,38]. Passive instruments (imagers and radiometers) deployed on low-elevation-orbit satellites provide global surveillance of clouds [39,40], while those installed on geostationary satellites provide continuous monitoring of cloudiness over large areas [41,42]. However, since the instruments are downward-looking, they are more suitable for determining the cloud top than the cloud base, and low clouds sometimes remain hidden [43,44]. In contrast, satellite-borne active profilers such as radars [45] and lidars [46] provide unique insights into cloud vertical structure with exceptional resolution [47]. Nonetheless, the temporal resolution of their products is hindered by the lengthy repeat cycle of polar-orbiting satellites, impeding diurnal cycle analyses [48]. Furthermore, atmospheric reanalysis datasets also provide cloud-related variables, but must be utilized with caution due to their inherent uncertainties [49,50].

The objective of this research is to ascertain the potential urban influences on cloud characteristics over Sofia and to quantify these effects. Additionally, the study aims to provide a comprehensive explanation for the observed phenomena. Furthermore, the investigation delves into analyzing the seasonal and diurnal variations in urban impact on cloud characteristics. In the subsequent section, we introduce the measurement sites and the atmospheric parameters utilized, alongside additional sources of data such as satellite products and atmospheric reanalysis. Section 3 encompasses a thorough analysis of the available data, exploring and evaluating the urban impact on cloud characteris-

tics. It is followed by discussions of key findings and conclusions in the final section of the manuscript.

2. Materials and Methods

2.1. Study Area, Instrumentations, and Sources of Data

This study integrates in situ and remote sensing measurements of cloud-related parameters at three locations (see Figure 1) alongside satellite data and atmospheric reanalysis spanning a decade-long period (2011–2020) across the city of Sofia, Bulgaria, and its surroundings. Situated within a valley oriented in a nearly northwest-to-southeast direction, Sofia is flanked by the Vitosha and Balkan Mountains.

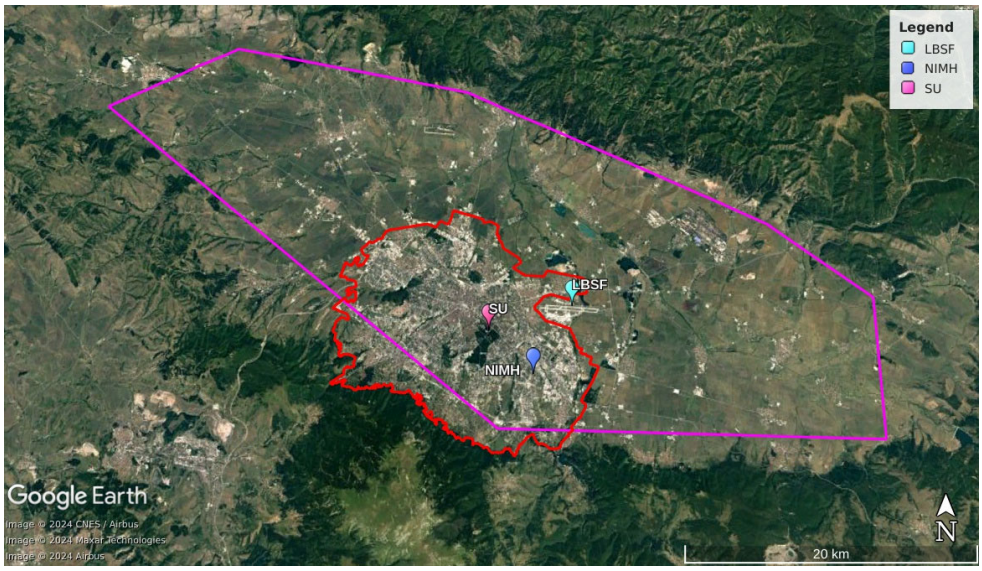

Figure 1. Sofia valley and the locations of LBSF (cyan), NIMH (blue) and SU (pink). The city building boundaries are depicted by a red polyline; the magenta polyline is the valley. Rural area is denoted by difference between the magenta and the red polygons.

The first location, Sofia Airport (hereafter denoted as LBSF), situated northeast of the city at the coordinates 42.696°N, 23.417°E and elevation 531 m above sea level (ASL), is equipped with instruments measuring meteorological variables that are critical for aviation safety. The airport's automated system records data at 30-min intervals, which are reported in Meteorological Aerodrome Reports (METAR). Atmospheric pressure, air temperature, and humidity (used in LCL estimation), as well as cloud base height (derived from a Vaisala CL31 ceilometer), are the selected parameters examined in this study.

The second site is situated within the largest urban park (hereinafter denoted as SU). The station has coordinates 42.682°N and 23.345°E, and an elevation 575 m ASL. This location is equipped with an automatic weather station (AWS) and a Lufft's ceilometer (CHM15k), which record data at intervals of 10 min and 1 min, respectively.

The present study utilizes CBH values (expressed in meters above the surface) reported by Lufft (CHM15k) and Vaisala (CL31) ceilometers. It is important to note that CBH data sourced from METAR reports may have undergone manual adjustments by observers to enhance the accuracy of the representation of cloudiness over the airport's vicinity. Given that the estimated height of the atmospheric boundary layer above Sofia during the summer season is approximately 2500 m [51], and also the fact that CBH values in the LBSF METAR are limited to this height, all ceilometers' records of higher clouds that were less likely to be related to the urban area influence were filtered out. Furthermore, an assessment of cloud persistence is employed as an additional parameter to elucidate the urban impact on cloud cover. This metric is calculated as the ratio of detected low-level clouds to the total number of ceilometer measurements conducted at the chosen site.

The third location, the synoptic station Sofia of the National Institute of Meteorology and Hydrology (hereafter referred to as NIMH, coordinates 42.654°N and 23.383°E, 592 m above sea level), is located in the eastern sector of the city. The surrounding area of the station exhibits sparse urban development and predominantly features low vegetation and scattered tree coverage. Standard meteorological parameters are measured at the station every 3 h.

Measurement of the near-surface atmospheric variables, such as air temperature, relative humidity, and atmospheric pressure, enables the calculation of the LCL, often utilized as a proxy for CBH [52]. However, it should not be overlooked that LCL values are strongly dependent on the microclimatic conditions specific to the measurement station, potentially introducing biases into estimates of cloud base height.

Although both stations, SU and NIMH, are located within the built-up boundaries of the city (which justifies considering them urban), one must bear in mind that near-surface measurements of atmospheric variables there may hardly exhibit typical urban effects, as the sensors' footprint covers vegetated areas. Conversely, the LBSF weather station, although it is situated outside urban territory (tempting to classify as rural), unquestionably experiences the influence of relatively extensive asphalted or concreted surfaces, making it difficult to expect typical rural values of the measured near-surface atmospheric variables. On the other hand, when measuring an atmospheric variable at higher altitudes (e.g., low-level clouds or atmospheric boundary layer), the effects of very local surface inhomogeneities are blended and blurred, so the measured quantities represent "average" effects from a broader area. The latter suggests that the cloudiness information retrieved by the ceilometer in the city center is very likely to detect urban influence, while ceilometer measurements at the airport are likely to be influenced by the rural areas, except in the case of a southerly winds when the "signal" at the airport comes from the urban area.

The daily balloon sounding is conducted at 12 UTC (14 LT) at the National Institute of Meteorology and Hydrology (NIMH) to obtain upper-air measurements of relative humidity and temperature. In cloud base detection, a thresholds-based methodology (adapted from [32]) is applied to the relative humidity (RH) profiles. Initially, increased humidity layers (where RH > RH_{min}) are identified. Subsequently, if the RH within that layer exceeds RH_{min} + RH_{jump}, the lower boundary of the layer is designated as CBH. Through experimentation with varying values, it was determined that RH_{min} = 85% and RH_{jump} = 3% yielded the best agreement with ceilometer-derived CBH data at LBSF.

The third version of the Satellite Application Facility on Climate Monitoring (CM SAF) climate dataset, CLARA A3 [53], is also used in the study. The analysis leverages several daily mean products from CLARA, including cloud top pressure (CTP), cloud optical thickness (COT), cloud top phase (CPH), and fractional cloud cover (CFC); the latter is utilized as a probabilistic cloud mask. Notably, all products utilized in the study have a spatial resolution of 0.25° × 0.25°.

The present study also examines the low-level cloud cover (LCC), defined as the proportion of the sky obscured by clouds with a base height below 2500 m, as provided by the single-level European Copernicus Regional Reanalysis (CERRA) datasets [54]. Additionally, wind speed and direction at 700 hPa, sourced from the CERRA pressure level dataset [55], are used to evaluate the influence of synoptic background wind patterns on the urban impact of cloudiness. Both datasets feature a spatial resolution of 5.5 km × 5.5 km and a temporal resolution of 3 h.

The evaluation of urban impact on cloudiness, as derived from the CERRA and CLARA datasets, entails the aggregation of data within the urbanized zone (outlined in red in Figure 1) and subsequent comparison with the average data obtained from the remaining regions of the Sofia valley (designated as rural areas).

2.2. Software and Tools

A variety of free and open-source software, programming languages, and packages are utilized in this work. R version 4.3 [56], as well as many R packages, are used for data

collection (climate version1.0.4 [57] and ecmwfr version 1.5.0 [58]), preprocessing (ncdf4 version 1.21 [59] and tidyverse version 2.0.0 [60]), analysis (tidyverse version 2.0.0 [60], sf version 1.0-13 and stars version 0.6-1 [61]), and visualization (tidyverse version 2.0.0 [60] and openair version 2.17-0 [62]). Additionally, CDO version 2.0.5 [63] is utilized in CLARA data processing.

3. Results

3.1. Lifting Condensation Level (LCL)

Measurements of near-surface air thermodynamic variables (humidity, temperature, and pressure) at each location allow for the calculation of LCL, representing the altitude at which an adiabatically lifted air parcel reaches saturation. As depicted in Figure 2, the LCL exhibits a comparable pattern, with peak values (2108, 1458, and 1660 m at LBSF, NIMH, and SU, respectively) observed during the afternoon hours of August across all locations. A secondary maximum (a second-highest seasonal peak) is evident in April, while a local minimum is observed in May and June, attributed to higher storm frequency and increased relative humidity, which results in a decrease in the LCL. The magnitude of LCL variations is comparable between SU and NIMH, but notably larger at LBSF. Throughout the winter months, diurnal variations in LCL diminish significantly.

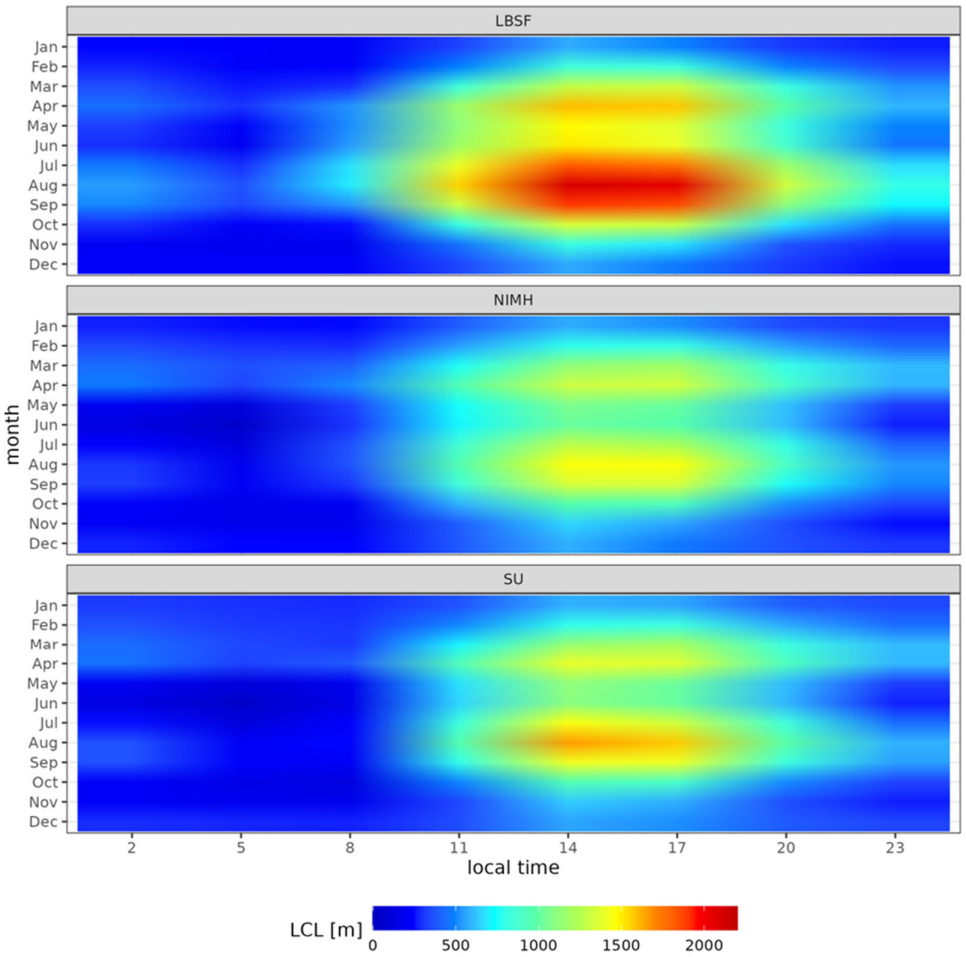

Figure 2. Diurnal and seasonal variations (heat map) of the mean LCL at LBSF, NIMH, and SU. The figure presents a summary of the dataset spanning the period from 2011 to 2020.

To shed more light on the observed differences in LCL between the SU and LBSF, the diurnal and seasonal variations of differences in air temperature, relative humidity, and LCL are presented as heatmaps in Figure 3. Statistically significant differences (*t*-test is conducted with *p*-value of 0.05) are indicated by circles. Notably, the LCL calculated for the

urban center (SU) is consistently lower than that for the airport (LBSF) during the warmer months, particularly in July and August, with maximal disparities reaching approximately −580 m, observed around 11 and 12 local time (LT). This contrast is mainly due to the higher relative humidity and slightly lower temperature at SU (see Figure 3), indicative of the distinctive microclimate within the urban park. Conversely, during nocturnal periods, particularly in colder seasons, the LCL difference approaches zero and even exhibits positive values. This phenomenon is attributed to the lower temperatures recorded at LBSF, resulting in higher relative humidity, and can potentially be attributed to the formation of a cool pool in the valley (given LBSF is the station with the lowest altitude).

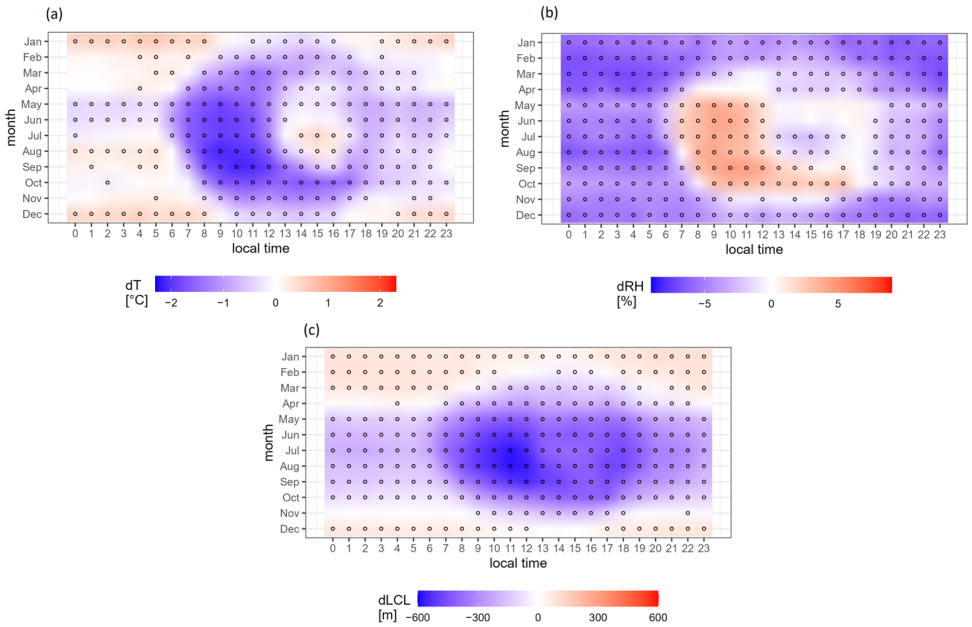

Figure 3. Heat maps of the mean difference in air temperature (**a**), relative humidity (**b**), and lifting condensation level (**c**) between SU and LBSF. Circles indicate statistically significant differences (conducted *t*-test with *p*-value 0.05). The figure presents a summary of the dataset spanning the period from 2011 to 2020.

3.2. Cloud Base Height (CBH) Determined by the Ceilometers

Figure 4 illustrates the diurnal and seasonal evolution of the mean cloud base height (CBH) over two distinct locations, SU and LBSF, as derived from ceilometer data. While exhibiting similar patterns, the two maxima appear slightly blurred and less distinct compared to those observed in LCL. Specifically, the ceilometer positioned in the city center (SU) registers higher CBH values relative to the one located at the northeastern periphery of the city (LBSF). The maximum mean CBH values of 1640 m and 1598 m were attained in August at 16:00 LT and 18:00 LT in SU and LBSF, respectively. Conversely, the minimum CBH values of 659 m and 594 m were calculated in February at 06:00 LT and December at 05:00 LT for SU and LBSF, respectively.

Figure 5 depicts the mean difference in CBH between the city center (SU) and Sofia Airport (LBSF), situated northeast of the city. The CBH values over SU are significantly (*t*-test with *p*-value 0.05 is conducted) higher than over LBSF in the summer months (the largest mean difference 286 m was estimated in May at 14 LT), but also during the winter months around midday, which may be attributed the urban influences. Conversely, during the early morning, late afternoon, and nighttime hours, CBH over the city center is generally lower than that over the airport (the lowest value −201 m is registered in February at 0 LT) (see Figure 5a). To assess the impact of the wind patterns on the observed CBH difference, wind data at 700 hPa level (approximately 3 km) sourced from the CERRA reanalysis are utilized. The CBH difference between SU and LBSF is computed across various wind speeds and directions and represented graphically on a polar diagram. The analysis reveals

that the CBH over the city center is higher than over the airport, indicating a positive difference, mainly when prevailing winds originate from the northwest, north, or northeast directions (see to Figure 5b). However, it is important to note that the bivariate polar plot (Figure 5b) does not account for wind frequency, rendering conclusions based solely on the apparent predominance of misleading negative CBH differences, as the region's wind rose predominantly features westerlies and northerly winds.

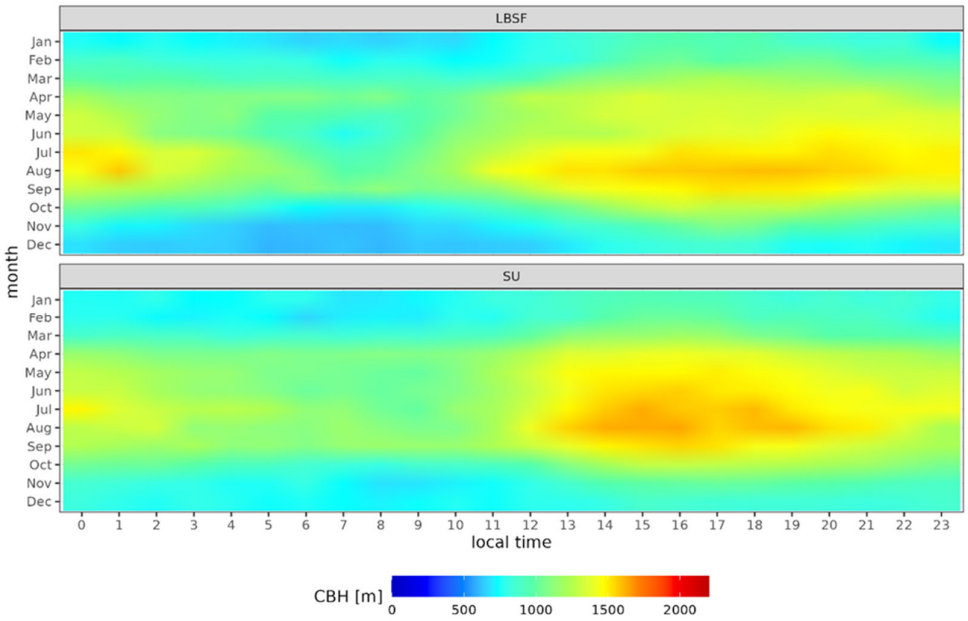

Figure 4. Diurnal and seasonal variations in the mean CBH of low-level clouds at LBSF and SU, respectively. The figure presents a summary of the dataset spanning the period from 2011 to 2020.

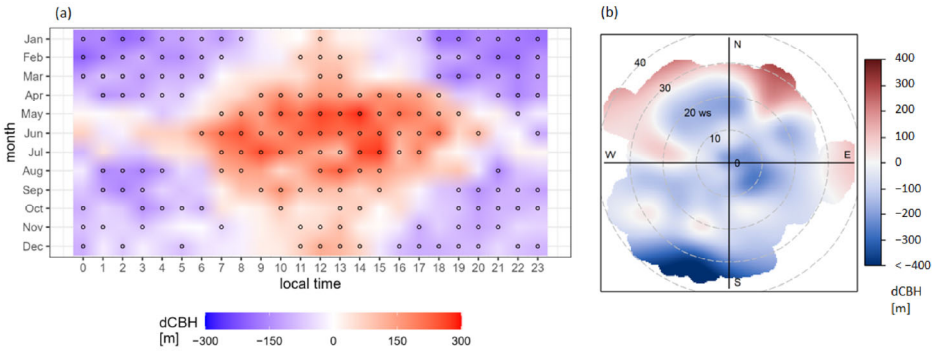

Figure 5. The mean difference in CBH (measured by the ceilometers) of low-level clouds (CBH < 2500 m) over SU (city center) and over LBSF (the airport at the city edge) as a heat map for different months and hours (**a**), where circles indicate statistically significant difference (*t*-test with *p*-value 0.05). A bivariate polar plot of the difference in CBH varying by wind speed (ws) and wind direction at 700 hPa (**b**). The figure presents a summary of the dataset spanning the period from 2011 to 2020.

3.3. Clouds Persistence Determined by the Ceilometers

Figure 6 shows the analogous diurnal–seasonal pattern of mean cloud persistence observed at both SU and LBSF sites. Specifically, cloud persistence during the spring and summer months exhibits a peak in the afternoon hours, which correlates with the development of convective clouds. Evidently, ceilometer observations indicate a lower likelihood of detecting low-level clouds over Sofia in August compared to other months, with the highest probability occurring during the winter season. Throughout the colder months, diurnal variations in cloud persistence are less pronounced, characterized primarily by

a nocturnal and early morning maximum, potentially indicative of low stratus clouds and fog formation.

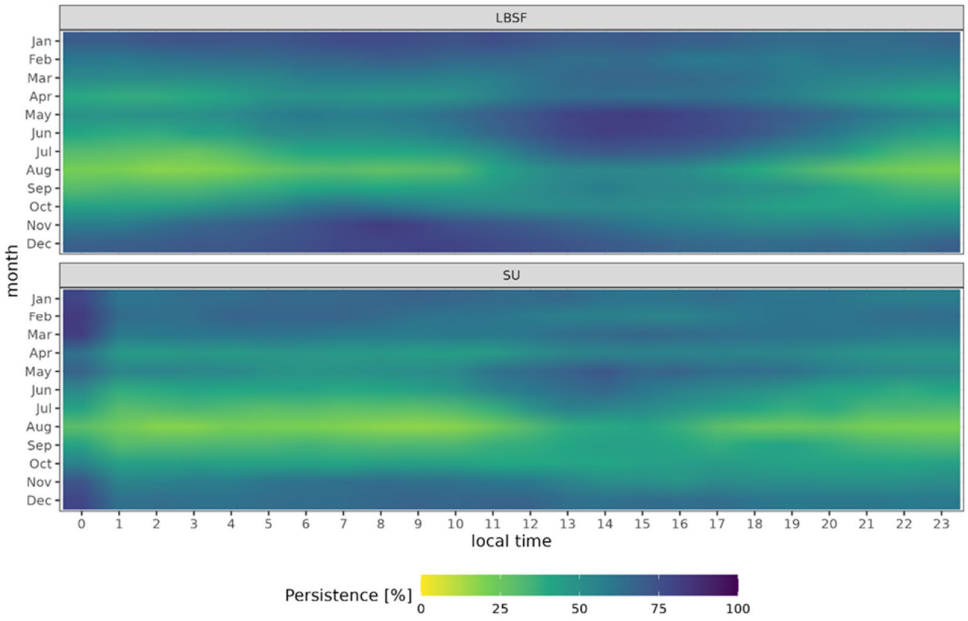

Figure 6. Diurnal and seasonal variations of the mean low-level cloud persistence at LBSF and SU, respectively. The figure presents a summary of the dataset spanning the period from 2011 to 2020.

The mean cloud persistence over the city center (SU) remains significantly lower (proportion test with p-value 0.05 is conducted) than that observed outside the urban area (LBSF) across a vast majority of instances. Specifically, during the afternoon hours of May, June, and July, the persistence difference reaches approximately −50% (see Figure 7a). Figure 7b reveals that the prevalence of low-level clouds over the city center (SU) compared to the airport (LBSF) is improbable, except under conditions of robust westerly (wind speed > 30 m/s) and northeasterly (wind speed > 20 m/s) winds at 700 hPa (wind data sourced from CERRA).

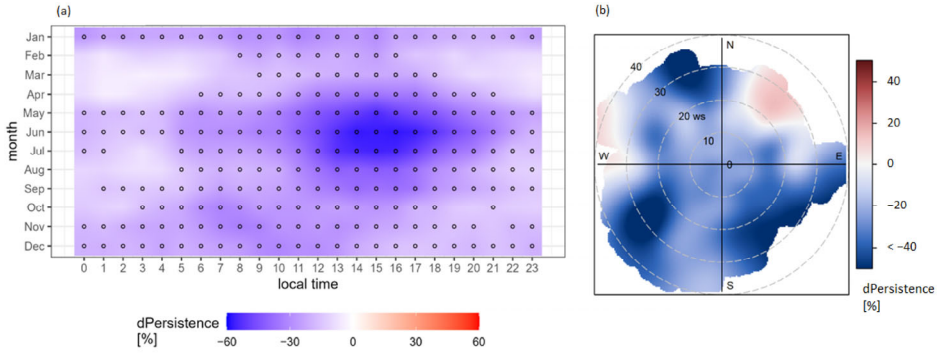

Figure 7. The mean difference in cloud persistence (measured by the ceilometers) of low clouds (CBH < 2500 m) at SU (city center) and LBSF (the airport at the city edge). A heat map for different months and hours (**a**), where circles indicate statistically significant (test of equal proportions at p-value 0.05) differences. A bivariate polar plot of the difference in cloud persistence varying by wind speed (ws) and wind direction at 700 hPa (**b**). The figure presents a summary of the dataset spanning the period from 2011 to 2020.

3.4. Validation of CBH Determined by the Rawinsonde

A sensitivity analysis and validation of rawinsonde-derived cloud base height (CBH) against ceilometers was conducted. The threshold values for minimum relative humidity (RH_{min}) and relative humidity jump (RH_{jump}) varied within the ranges of 80–88% and

2–6%, respectively. Our findings reveal a consistent underestimation of CBH values when compared to CHM15k ceilometers at SU, whereas compared to CL31 ceilometers at LBSF, the bias reaches a minimum (−8 m) at RH_{min} = 85% and RHj_{ump} = 3% (see Figure 8). While it may be tempting to attribute the observed bias of rawinsonde-derived CBH against the ceilometer in the city center to urban influences, it is crucial to take into account the use of different atmospheric profiles, such as relative humidity versus aerosol loading, which may result in discrepancies between CBH estimates.

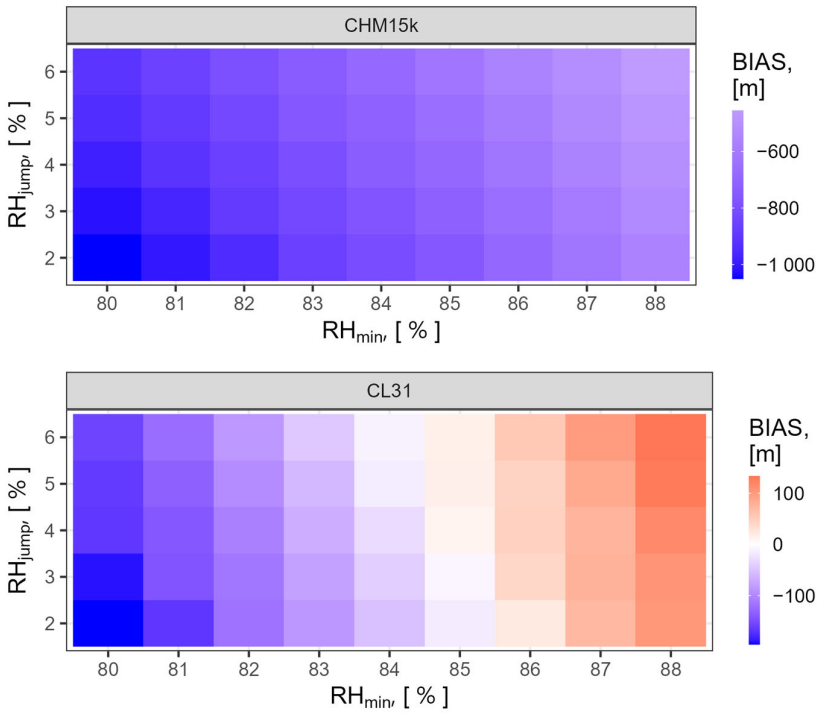

Figure 8. BIAS of CBH determined from rawinsonde RH profiles against CBH obtained by the ceilometers—CL31(at the airport) and CHM15k (in the city center) as a function of the method parameters RH_{min} and RH_{jump}. The figure presents a summary of the dataset spanning the period from 2011 to 2020.

3.5. Low-Level Cloud Cover (LCC) in CERRA

The low-level cloud cover over the Sofia valley exhibits somewhat patchy distribution, making it challenging to discern a distinct pattern or observe notable urban–rural contrasts (see Figure 9). However, a slight predominance of clouds is observed over the western and northern borders of the urbanized zone, while the cloud cover appears less dense in the central, eastern, and southern sectors of the city. This phenomenon may be attributed to prevailing westerly and northerly winds in the region. It is noteworthy that diurnal variations are largely absent in the dataset (not depicted).

The analysis of mean LCC disparities between urban and rural regions, as depicted in Figure 10a, indicates a lack of discernible urban influence within the CERRA dataset. Notably, the sole statistically significant difference of nearly −10% (determined via a proportion test with a *p*-value of 0.05) was observed in November at 23:00 LT. Additionally, Figure 10b illustrates that, while variations in LCC between urban and rural locales are generally modest, certain wind regimes exhibit a discernible influence, such as enhanced LCC over urban regions relative to their rural counterparts during easterly and northeasterly winds, resulting in LCC differences (dLCC) of several percentage points.

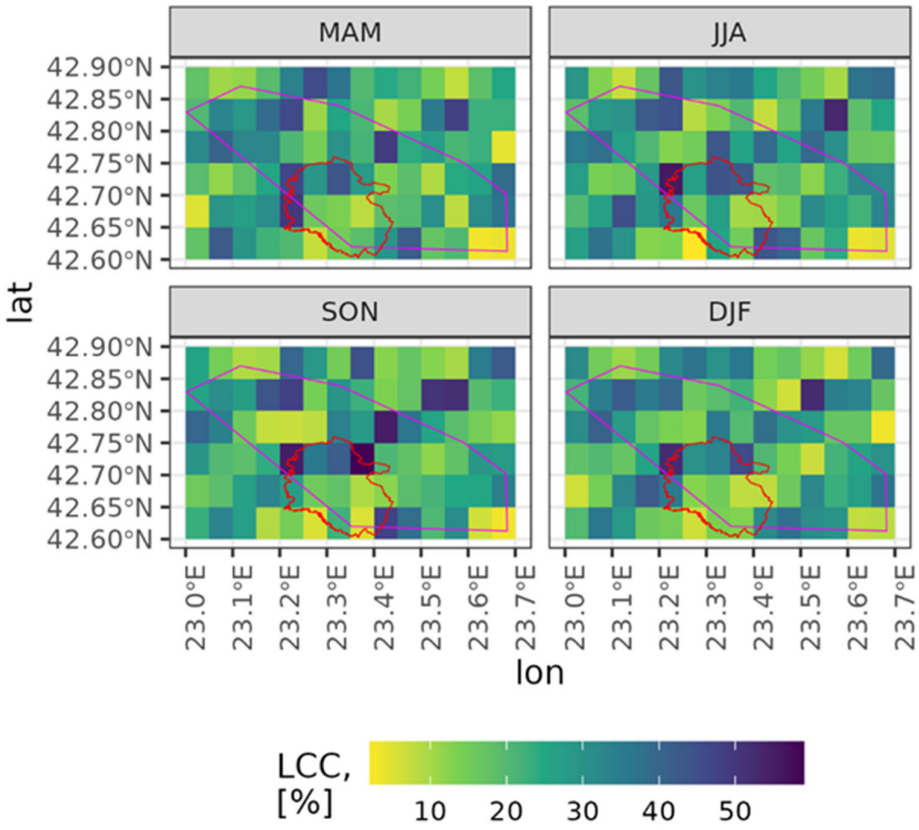

Figure 9. Seasonal variations in CERRA's LCC. The magenta and red polylines enclose the valley and built-up areas, respectively. The figure presents a summary of the dataset spanning the period from 2011 to 2020.

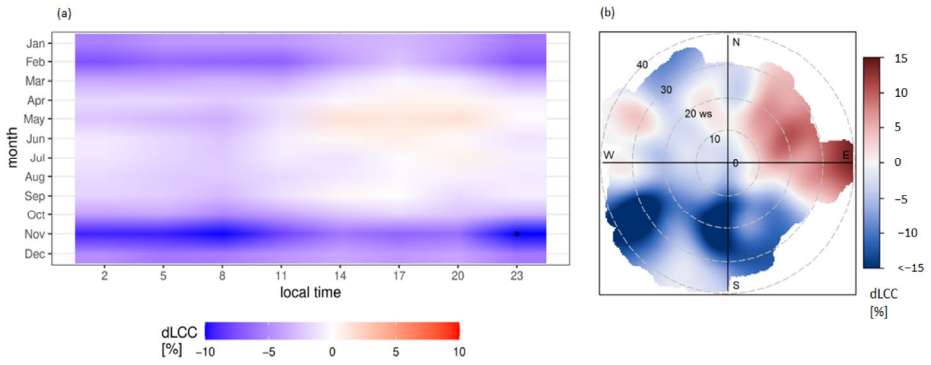

Figure 10. The mean difference in CERRA's low cloud cover (CBH < 2500 m) over the built-up area and over the rural area. A heat map for different months and hours (**a**), where circles indicate statistically significant (test of equal proportions at *p*-value 0.05) differences. A bivariate polar plot of the difference in LCC varying by wind speed (ws) and wind direction at 700 hPa (**b**). The figure presents a summary of the dataset spanning the period from 2011 to 2020.

3.6. Joint Cloud Histograms Based on CLARA Products

The joint cloud histograms (2D histogram of COT and CTP) for both urban and rural areas are depicted in Figure 11, categorized by season (MAM for spring, JJA for summer, SON for autumn, and DJF for winter) and the thermodynamic phases of particles at the cloud top (ice or liquid). Two discernible details potentially related to the urban influences on cloud dynamics are worth noting. Firstly, optically thin, low clouds (indicated by high pressure at the cloud top) extend to lower altitudes over rural areas compared to their urban counterparts, regardless of the water phase at the cloud top. These may be boundary layer-coupled thin clouds or fogs, and one can assume their formation is less frequent and/or

at a slightly higher altitude over the urban area as a result of more intense updrafts and a dryer atmosphere above the city. Secondly, there is a notable decrease in the presence of optically thick clouds, particularly during the spring and summer months, over rural areas compared to urban environments. This discrepancy may suggest enhanced convective activity and the intensification of convective storms over urban areas, potentially driven by more vigorous updrafts.

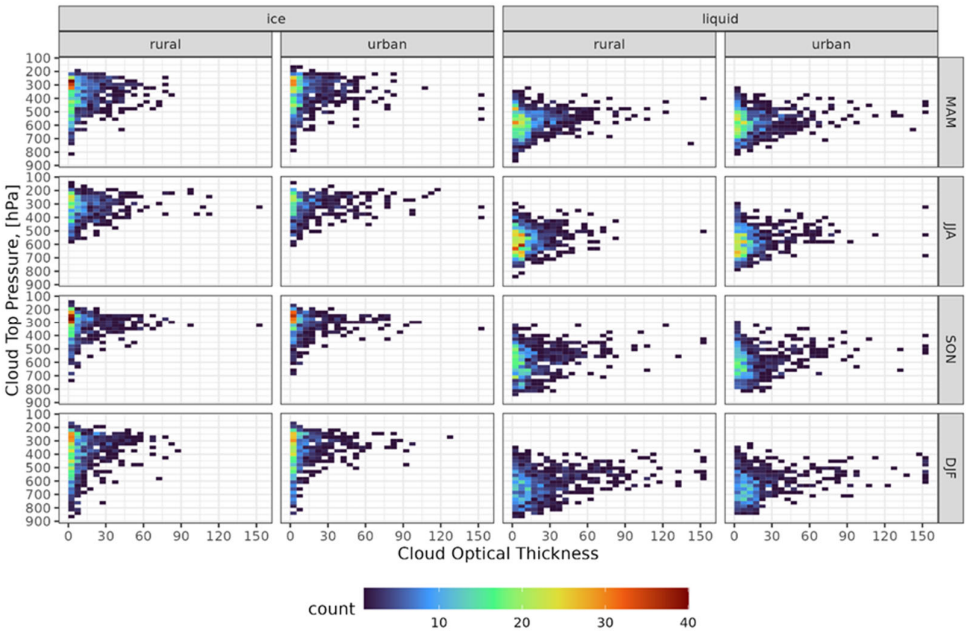

Figure 11. COT-CTP histograms for ice cloud top (**left side**) and water cloud top (**right side**) clouds detected over the rural and urban areas, respectively, during different seasons (MAM—spring, JJA—summer, SON—autumn, DJF—winter). The figure presents a summary of the dataset spanning the period from 2011 to 2020.

Examination of the probabilistic cloud mask derived from CLARA data revealed no statistically significant disparity (as confirmed by the Kolmogorov-Smirnov test) in the empirical cloud cover distributions between urban and rural locales. The absence of an urban signal is attributed to the inclusion of not only low-level clouds, but also mid- and high-level cloud formations within the mask.

4. Discussion

It is widely acknowledged that differences in atmospheric variables between urban and rural regions are most discernible during fair weather conditions, particularly when the urban heat island phenomenon is most pronounced. The influence of urbanization on cloud formation and characteristics is contingent upon various factors, including the size and morphology of the urban area, surface characteristics, and synoptic-scale atmospheric forcing [64,65]. Additionally, topography effects on cloud cover have also been reported [66]. Finally, the effects of urbanization on cloudiness exhibit diurnal and seasonal variations, which may appear differently across diverse climatic regimes.

The LCL presents an appealing option for determining CBH and its spatiotemporal dynamics due to its modest data requirements [52]. However, it is primarily applicable under convective conditions, and even then, the entrainment of ambient air by the rising air parcel is difficult to account for. Moreover, the sensors' locations and exposition may result in sampling vastly different and unrepresentative local climate conditions, potentially yielding unexpected outcomes, particularly in the presence of local heat and/or water vapor sources. Furthermore, LCL estimates based on near-surface data may underestimate the actual height of the cloud base, whereas the mean-air parcel (first 100 hPa) provides a more representative metric for convection-related phenomena [67].

Although ceilometers serve as a reference instrument for measuring CBH, the utilization of ceilometers from various manufacturers may introduce systematic discrepancies in the derived CBH values [68]. Such differences may emerge even after firmware updates to a given instrument. Another source of uncertainty that may influence the results is the weather observer, who can adjust the ceilometer's data to be more representative for the area. Nonetheless, Martucci et al. [68] observed a tendency of Vaisala's product (in our case, at LBSF) to indicate a slightly higher CBH compared to Lufft's product (located in the city center), which at least partially substantiates the credibility of the urban influence identified in our study. Additionally, other studies have also reported an increase in CBH over urban areas [69]. The uncertainty in ceilometer cloud detection algorithms may also affect the observed differences in cloud persistence. In this study, it was found that clouds over the city center exhibit reduced persistence relative to those over the airport (located outside the city), which contradicts results reported by other authors [13]. This inconsistency may be influenced by factors such as the scale of the studied urban areas (Sofia is smaller than mega-cities like London or Paris). Additionally, the choice of the upper limit of CBH values, which define clouds subject to urbanization impacts, may contribute to the observed inconsistency. For example, while this study considered CBH values up to 2500 m, another study extended this limit to 3000 m [13]. Consequently, it is plausible to suggest that these threshold values should be tailored to the specific study sites, potentially accounting for seasonal variations to accurately capture the relationship between low-level clouds and the urban boundary layer.

The validation of CBH derived from radiosonde RH profiles revealed threshold values consistent with those reported in the literature [70], particularly when compared against the ceilometer located in the city's periphery. Notably, the ceilometer positioned in the city center consistently recorded higher CBH values relative to those derived from radiosonde data, a phenomenon potentially attributable to urbanization-induced alterations in cloud dynamics. However, this discrepancy may be attributed to the different profiles utilized by the respective instruments (relative humidity vs. aerosol loading). Furthermore, it is conceivable that wind-induced displacement of the rawinsonde during ascent, or its traversal to the periphery of the cloud due to updraft divergence, may introduce additional uncertainties into the findings.

In the CERRA reanalysis, the lack of statistically significant differences observed between urban and rural LCC may be attributed to the coarse spatial resolution employed and/or the deficiencies in urban processes parameterizations. Moreover, the representation of cloud cover in the reanalyses may be biased [71]. Future investigations focusing on megacities and utilizing improved reanalysis datasets have the potential to contribute to the refinement of our comprehension regarding the influence of urbanization on local weather and climate dynamics, particularly with respect to cloud cover.

Despite the coarse spatial resolution of the CLARA's products, analyses of COT-CTP histograms reveal discernible differences in cloud characteristics between urban and rural areas. Specifically, optically thin, low-level cloud tops are higher over the urban region compared to rural areas. Additionally, there are some indications of convection intensifications over the city during the spring–summer period, characterized by the presence of optically thick clouds that are likely influenced by thermally driven updrafts and surface wind convergence. However, it is essential to note that such observations may be influenced by area averaging effects, as convective storm may cover larger parts of the city, but it is not so likely to cover the entire valley. Consequently, further investigations are required to corroborate these findings across various urban settings, encompassing both small towns and megacities in regions with varied rural landscapes across different climatic conditions.

5. Conclusions

A variety of data sources, including in situ measurements, ceilometer profiles, radiosonde profiles, satellite products, and atmospheric reanalyses, have been used to elucidate and quantify the urbanization impact on cloud's characteristics over Sofia, Bulgaria.

The diurnal–seasonal distribution of LCL across all stations exhibits a bimodal pattern, with peaks observed in the afternoons of April and August. The station located outside the urban area records the highest mean LCL value (2100 m), whereas the mean values at the two other stations within the eastern and central urban sectors are notably lower (1500–1600 m). This unexpected outcome is due to the methodological constraint whereby calculated values are heavily influenced by the local microclimate surrounding each weather station. The local minimum registered in May–June at all stations is attributed to stormy weather conditions characterized by increased precipitation.

The analysis of ceilometer data showed that over the central urban regions, the mean CBH attains 1640 m, demonstrating approximately 200 m greater values during warm seasons and daylight hours compared to CBH values registered at the airport. The higher CBH over the city center compared to the periphery is accompanied mainly by westerly and northerly winds in the free atmosphere, which prevail for the region. Moreover, clouds observed over the urban center are found to be less persistent than those observed over the airport, with differences of up to 50% noted during summer afternoons.

The utilization of a threshold approach to radiosonde relative humidity profiles reveals unbiased results in CBH retrieval when compared to the ceilometer at the airport. However, there is a systematic underestimation observed in comparison to the ceilometer situated in the city center.

LCC data obtained from CERRA did not reveal significant distinctions between urban and rural areas. However, an augmentation in cloud coverage was noted along the western and northern edges of the urban area, corresponding to prevailing wind patterns in the region.

Analysis of 2D histograms of COT and CTP reveals that the low-level, optically thin clouds over the urban areas exhibit marginally higher tops, possibly indicative of a slightly elevated condensation level over the city. Additionally, the histograms reveal an increased frequency of the optically thickest clouds over urban areas compared to rural regions, which can likely be attributed to the intensified convective activity over urban areas resulting from thermal and dynamic enhancement of updrafts.

The presented results provide promising indications suggesting that urbanization influences cloudiness in Sofia, Bulgaria. Moreover, these findings offer insights into the influence of urban areas on some cloud properties. It is worth noting the relative proximity of Sofia Airport to the city center, so one might expect differences in the magnitudes of the urban influence found when analyzing other locations. It is advisable to conduct analogous investigations in other cities characterized by various sizes, urban structures, and urban rhythms, situated in diverse climatic regions and surrounded by various rural landscapes. Such endeavors will deepen our comprehension of the interactions between urban environments and cloud cover.

Funding: This research was funded by the Bulgarian National Science Fund, grant number KP-06-COST/7 from 19 August 2021.

Data Availability Statement: Almost all datasets analyzed in this study are publicly available. METAR data are freely available at https://mesonet.agron.iastate.edu/ (accessed on 25 April 2023). The near-surface synoptic observations are freely available at https://www.ogimet.com/ (accessed on 13 May 2023). The rawinsonde profiles can be downloaded from http://weather.uwyo.edu/upperair/sounding.html (accessed on 19 May 2023). Copernicus Climate Change Service of ECMWF provides access to CERRA datasets at https://cds.climate.copernicus.eu (accessed on 24 May 2023). CLARA-A3 dataset can be obtained from the Satellite Application Facility on Climate Monitoring (CM SAF) at https://doi.org/10.5676/EUM_SAF_CM/CLARA_AVHRR/V003 (accessed on 13 June 2023). The dataset from SU station is available from the author upon request.

Acknowledgments: This work was carried out in the framework of the National Science Program "Environmental Protection and Reduction of Risks of Adverse Events and Natural Disasters", approved by the Resolution of the Council of Ministers No. 577/17.08.2018 and supported by the Ministry of Education and Science (MES) of Bulgaria (Agreement No. D01-27/06.02.2024). This publication is also based upon work within COST Action PROBE CA18235, supported by COST (European Cooperation in Science and Technology). It is imperative to acknowledge the significant assistance provided by Danko Ivanov in the operation and maintenance of the weather station and ceilometer at the SU station. The anonymous reviewers deserve acknowledgement for their comments, which led to the improvement of the manuscript.

Conflicts of Interest: The author declares no conflicts of interest.

References

1. Bony, S.; Stevens, B.; Frierson, D.M.W.; Jakob, C.; Kageyama, M.; Pincus, R.; Shepherd, T.G.; Sherwood, S.C.; Siebesma, A.P.; Sobel, A.H.; et al. Clouds, Circulation and Climate Sensitivity. *Nature Geosci.* **2015**, *8*, 261–268. [CrossRef]
2. Zelinka, M.D.; Hartmann, D.L. Why Is Longwave Cloud Feedback Positive? *J. Geophys. Res.* **2010**, *115*, D16117. [CrossRef]
3. Hartmann, D.L.; Ockert-Bell, M.E.; Michelsen, M.L. The Effect of Cloud Type on Earth's Energy Balance: Global Analysis. *J. Climate* **1992**, *5*, 1281–1304. [CrossRef]
4. Allan, R.P.; Barlow, M.; Byrne, M.P.; Cherchi, A.; Douville, H.; Fowler, H.J.; Gan, T.Y.; Pendergrass, A.G.; Rosenfeld, D.; Swann, A.L.S.; et al. Advances in Understanding Large-Scale Responses of the Water Cycle to Climate Change. *Ann. N. Y. Acad. Sci.* **2020**, *1472*, 49–75. [CrossRef] [PubMed]
5. Barbieri, F.; Rajakaruna, S.; Ghosh, A. Very Short-Term Photovoltaic Power Forecasting with Cloud Modeling: A Review. *Renew. Sustain. Energy Rev.* **2017**, *75*, 242–263. [CrossRef]
6. Bocheva, L.; Dimitrova, T.; Penchev, R.; Gospodinov, I.; Simeonov, P. Severe Convective Supercell Outbreak over Western Bulgaria on July 8, 2014. *Idojaras* **2018**, *122*, 177–203. [CrossRef]
7. Yau, M.K.; Rogers, R.R. *A Short Course in Cloud Physics*; Elsevier: Amsterdam, The Netherlands, 1996; ISBN 978-0-08-057094-5.
8. Guo, X.; Fu, D.; Wang, J. Mesoscale Convective Precipitation System Modified by Urbanization in Beijing City. *Atmos. Res.* **2006**, *82*, 112–126. [CrossRef]
9. Liu, J.; Niyogi, D. Meta-Analysis of Urbanization Impact on Rainfall Modification. *Sci. Rep.* **2019**, *9*, 7301. [CrossRef]
10. Li, Y.; Fowler, H.J.; Argüeso, D.; Blenkinsop, S.; Evans, J.P.; Lenderink, G.; Yan, X.; Guerreiro, S.B.; Lewis, E.; Li, X. Strong Intensification of Hourly Rainfall Extremes by Urbanization. *Geophys. Res. Lett.* **2020**, *47*, e2020GL088758. [CrossRef]
11. Danchovski, V.; Ivanov, D. Urban Effects on Cloud Base Height and Cloud Persistence over Sofia, Bulgaria Environ. *Sci. Proc.* **2024**, *29*, 45. [CrossRef]
12. Angevine, W.M.; White, A.B.; Senff, C.J.; Trainer, M.; Banta, R.M.; Ayoub, M.A. Urban–Rural Contrasts in Mixing Height and Cloudiness over Nashville in 1999. *J. Geophys. Res. Atmos.* **2003**, *108*. [CrossRef]
13. Theeuwes, N.E.; Barlow, J.F.; Teuling, A.J.; Grimmond, C.S.B.; Kotthaus, S. Persistent Cloud Cover over Mega-Cities Linked to Surface Heat Release. *npj Clim. Atmos. Sci.* **2019**, *2*, 15. [CrossRef]
14. Lemonsu, A.; Masson, V. Simulation of a Summer Urban Breeze Over Paris. *Bound. -Layer Meteorol.* **2002**, *104*, 463–490. [CrossRef]
15. Han, J.-Y.; Baik, J.-J. A Theoretical and Numerical Study of Urban Heat Island–Induced Circulation and Convection. *J. Atmos. Sci.* **2008**, *65*, 1859–1877. [CrossRef]
16. Varentsov, M.; Wouters, H.; Platonov, V.; Konstantinov, P. Megacity-Induced Mesoclimatic Effects in the Lower Atmosphere: A Modeling Study for Multiple Summers over Moscow, Russia. *Atmosphere* **2018**, *9*, 50. [CrossRef]
17. Rozoff, C.M.; Cotton, W.R.; Adegoke, J.O. Simulation of St. Louis, Missouri, Land Use Impacts on Thunderstorms. *J. Appl. Meteorol. Climatol.* **2003**, *42*, 716–738. [CrossRef]
18. Han, J.-Y.; Baik, J.-J.; Lee, H. Urban Impacts on Precipitation. *Asia-Pac. J. Atmos. Sci.* **2014**, *50*, 17–30. [CrossRef]
19. Huang, T.; Yim, S.H.; Yang, Y.; Lee, O.S.; Lam, D.H.; Cheng, J.C.; Guo, J. Observation of Turbulent Mixing Characteristics in the Typical Daytime Cloud-Topped Boundary Layer over Hong Kong in 2019. *Remote Sens.* **2020**, *12*, 1533. [CrossRef]
20. Rosenfeld, D. Suppression of Rain and Snow by Urban and Industrial Air Pollution. *Science* **2000**, *287*, 1793–1796. [CrossRef]
21. Mochida, M.; Kuwata, M.; Miyakawa, T.; Takegawa, N.; Kawamura, K.; Kondo, Y. Relationship between Hygroscopicity and Cloud Condensation Nuclei Activity for Urban Aerosols in Tokyo. *J. Geophys. Res. Atmos.* **2006**, *111*. [CrossRef]
22. Zhang, Q.; Quan, J.; Tie, X.; Huang, M.; Ma, X. Impact of Aerosol Particles on Cloud Formation: Aircraft Measurements in China. *Atmos. Environ.* **2011**, *45*, 665–672. [CrossRef]
23. Han, J.-Y.; Baik, J.-J.; Khain, A.P. A Numerical Study of Urban Aerosol Impacts on Clouds and Precipitation. *J. Atmos. Sci.* **2012**, *69*, 504–520. [CrossRef]
24. Schmid, P.E.; Niyogi, D. Modeling Urban Precipitation Modification by Spatially Heterogeneous Aerosols. *J. Appl. Meteorol. Climatol.* **2017**, *56*, 2141–2153. [CrossRef]
25. Zhong, S.; Qian, Y.; Zhao, C.; Leung, R.; Yang, X.-Q. A Case Study of Urbanization Impact on Summer Precipitation in the Greater Beijing Metropolitan Area: Urban Heat Island versus Aerosol Effects. *J. Geophys. Res. Atmos.* **2015**, *120*, 10903–10914. [CrossRef]

26. Kingfield, D.M.; Calhoun, K.M.; De Beurs, K.M.; Henebry, G.M. Effects of City Size on Thunderstorm Evolution Revealed through a Multiradar Climatology of the Central United States. *J. Appl. Meteorol. Climatol.* **2018**, *57*, 295–317. [CrossRef]
27. Dou, J.; Wang, Y.; Bornstein, R.; Miao, S. Observed Spatial Characteristics of Beijing Urban Climate Impacts on Summer Thunderstorms. *J. Appl. Meteorol. Climatol.* **2015**, *54*, 94–105. [CrossRef]
28. Ryu, Y.-H.; Baik, J.-J.; Han, J.-Y. Daytime Urban Breeze Circulation and Its Interaction with Convective Cells. *Q. J. R. Meteorol. Soc.* **2013**, *139*, 401–413. [CrossRef]
29. Theeuwes, N.E.; Boutle, I.A.; Clark, P.A.; Grimmond, S. Understanding London's Summertime Cloud Cover. *Q. J. R. Meteorol. Soc.* **2022**, *148*, 454–465. [CrossRef]
30. Mittermaier, M. A Critical Assessment of Surface Cloud Observations and Their Use for Verifying Cloud Forecasts. *Q. J. R. Meteorol. Soc.* **2012**, *138*, 1794–1807. [CrossRef]
31. Lawrence, M.G. The Relationship between Relative Humidity and the Dewpoint Temperature in Moist Air: A Simple Conversion and Applications. *Bull. Am. Meteorol. Soc.* **2005**, *86*, 225–234. [CrossRef]
32. Poore, K.D.; Wang, J.; Rossow, W.B. Cloud Layer Thicknesses from a Combination of Surface and Upper-Air Observations. *J. Clim.* **1995**, *8*, 550–568. [CrossRef]
33. Comstock, J.M.; Ackerman, T.P.; Mace, G.G. Ground-Based Lidar and Radar Remote Sensing of Tropical Cirrus Clouds at Nauru Island: Cloud Statistics and Radiative Impacts. *J. Geophys. Res. Atmos.* **2002**, *107*, AAC 16-1–AAC 16-14. [CrossRef]
34. Gryning, S.-E.; Batchvarova, E.; Floors, R.; Münkel, C.; Skov, H.; Sørensen, L.L. Observed and Modelled Cloud Cover up to 6 km Height at Station Nord in the High Arctic. *Int. J. Climatol.* **2021**, *41*, 1584–1598. [CrossRef]
35. Pîrloagă, R.; Ene, D.; Boldeanu, M.; Antonescu, B.; O'Connor, E.J.; Ştefan, S. Ground-Based Measurements of Cloud Properties at the Bucharest–Măgurele Cloudnet Station: First Results. *Atmosphere* **2022**, *13*, 1445. [CrossRef]
36. An, N.; Pinker, R.T.; Wang, K.; Rogers, E.; Zuo, Z. Evaluation of Cloud Base Height in the North American Regional Reanalysis Using Ceilometer Observations. *Int. J. Climatol.* **2020**, *40*, 3161–3178. [CrossRef]
37. Illingworth, A.J.; Cimini, D.; Haefele, A.; Haeffelin, M.; Hervo, M.; Kotthaus, S.; Löhnert, U.; Martinet, P.; Mattis, I.; O'Connor, E.J.; et al. How Can Existing Ground-Based Profiling Instruments Improve European Weather Forecasts? *Bull. Am. Meteorol. Soc.* **2019**, *100*, 605–619. [CrossRef]
38. Cimini, D.; Haeffelin, M.; Kotthaus, S.; Löhnert, U.; Martinet, P.; O'Connor, E.; Walden, C.; Coen, M.C.; Preissler, J. Towards the Profiling of the Atmospheric Boundary Layer at European Scale—Introducing the COST Action PROBE. *Bull. Atmos. Sci. Technol.* **2020**, *1*, 23–42. [CrossRef]
39. Platnick, S.; King, M.D.; Ackerman, S.A.; Menzel, W.P.; Baum, B.A.; Riedi, J.C.; Frey, R.A. The MODIS Cloud Products: Algorithms and Examples from Terra. *IEEE Trans. Geosci. Remote Sens.* **2003**, *41*, 459–473. [CrossRef]
40. Pavolonis, M.J.; Heidinger, A.K. Daytime Cloud Overlap Detection from AVHRR and VIIRS. *J. Appl. Meteorol. Climatol.* **2004**, *43*, 762–778. [CrossRef]
41. Derrien, M.; Le Gléau, H. MSG/SEVIRI Cloud Mask and Type from SAFNWC. *Int. J. Remote Sens.* **2005**, *26*, 4707–4732. [CrossRef]
42. Yang, Y.; Zhao, C.; Fan, H. Spatiotemporal Distributions of Cloud Properties over China Based on Himawari-8 Advanced Himawari Imager Data. *Atmos. Res.* **2020**, *240*, 104927. [CrossRef]
43. Amato, U.; Antoniadis, A.; Cuomo, V.; Cutillo, L.; Franzese, M.; Murino, L.; Serio, C. Statistical Cloud Detection from SEVIRI Multispectral Images. *Remote Sens. Environ.* **2008**, *112*, 750–766. [CrossRef]
44. Stubenrauch, C.J.; Rossow, W.B.; Kinne, S.; Ackerman, S.; Cesana, G.; Chepfer, H.; Girolamo, L.D.; Getzewich, B.; Guignard, A.; Heidinger, A.; et al. Assessment of Global Cloud Datasets from Satellites: Project and Database Initiated by the GEWEX Radiation Panel. *Bull. Am. Meteorol. Soc.* **2013**, *94*, 1031–1049. [CrossRef]
45. Stephens, G.L.; Vane, D.G.; Boain, R.J.; Mace, G.G.; Sassen, K.; Wang, Z.; Illingworth, A.J.; O'connor, E.J.; Rossow, W.B.; Durden, S.L.; et al. THE CLOUDSAT MISSION AND THE A-TRAIN: A New Dimension of Space-Based Observations of Clouds and Precipitation. *Bull. Am. Meteorol. Soc.* **2002**, *83*, 1771–1790. [CrossRef]
46. Winker, D.M.; Pelon, J.R.; McCormick, M.P. CALIPSO Mission: Spaceborne lidar for observation of aerosols and clouds. In Proceedings of the Lidar Remote Sensing for Industry and Environment Monitoring III, Hangzhou, China, 23–27 October 2002; SPIE: Washington, DC, USA, 2003; Volume 4893, pp. 1–11.
47. Rossow, W.B.; Zhang, Y. Evaluation of a Statistical Model of Cloud Vertical Structure Using Combined CloudSat and CALIPSO Cloud Layer Profiles. *J. Clim.* **2010**, *23*, 6641–6653. [CrossRef]
48. Stephens, G.; Winker, D.; Pelon, J.; Trepte, C.; Vane, D.; Yuhas, C.; L'Ecuyer, T.; Lebsock, M. CloudSat and CALIPSO within the A-Train: Ten Years of Actively Observing the Earth System. *Bull. Am. Meteorol. Soc.* **2018**, *99*, 569–581. [CrossRef]
49. Dolinar, E.K.; Dong, X.; Xi, B. Evaluation and Intercomparison of Clouds, Precipitation, and Radiation Budgets in Recent Reanalyses Using Satellite-Surface Observations. *Clim. Dyn.* **2016**, *46*, 2123–2144. [CrossRef]
50. Yao, B.; Teng, S.; Lai, R.; Xu, X.; Yin, Y.; Shi, C.; Liu, C. Can Atmospheric Reanalyses (CRA and ERA5) Represent Cloud Spatiotemporal Characteristics? *Atmos. Res.* **2020**, *244*, 105091. [CrossRef]
51. Danchovski, V. Summertime Urban Mixing Layer Height over Sofia, Bulgaria. *Atmosphere* **2019**, *10*, 36. [CrossRef]
52. Romps, D.M. Exact Expression for the Lifting Condensation Level. *J. Atmos. Sci.* **2017**, *74*, 3891–3900. [CrossRef]
53. Karlsson, K.-G.; Stengel, M.; Meirink, J.F.; Riihelä, A.; Trentmann, J.; Akkermans, T.; Stein, D.; Devasthale, A.; Eliasson, S.; Johansson, E.; et al. CLARA-A3: The Third Edition of the AVHRR-Based CM SAF Climate Data Record on Clouds, Radiation and Surface Albedo Covering the Period 1979 to 2023. *Earth Syst. Sci. Data* **2023**, *15*, 4901–4926. [CrossRef]

54. Schimanke, S.; Ridal, M.; Le Moigne, P.; Berggren, L.; Undén, P.; Randriamampianina, R.; Andrea, U.; Bazile, E.; Bertelsen, A.; Brousseau, P.; et al. CERRA Sub-Daily Regional Reanalysis Data for Europe on Single Levels from 1984 to Present. Available online: https://cds.climate.copernicus.eu/cdsapp#!/dataset/10.24381/cds.622a565a?tab=overview(accessed on 24 May 2023).
55. Schimanke, S.; Ridal, M.; Le Moigne, P.; Berggren, L.; Undén, P.; Randriamampianina, R.; Andrea, U.; Bazile, E.; Bertelsen, A.; Brousseau, P.; et al. CERRA Sub-Daily Regional Reanalysis Data for Europe on Pressure Levels from 1984 to Present. Available online: https://cds.climate.copernicus.eu/cdsapp#!/dataset/10.24381/cds.a39ff99f?tab=overview(accessed on 24 May 2023).
56. R Core Team. *R: A Language and Environment for Statistical Computing*; R Foundation for Statistical Computing: Vienna, Austria, 2023.
57. Czernecki, B.; Głogowski, A.; Nowosad, J. Climate: An R Package to Access Free In-Situ Meteorological and Hydrological Datasets For Environmental Assessment. *Sustainability* **2020**, *12*, 394. [CrossRef]
58. Hufkens, K.; Stauffer, R.; Campitelli, E. The Ecwmfr Package: An Interface to ECMWF API Endpoints. Available online: https://zenodo.org/records/7004985(accessed on 15 May 2023).
59. Pierce, D. Ncdf4: Interface to Unidata netCDF (Version 4 or Earlier) Format Data Files. Available online: https://cirrus.ucsd.edu/~pierce/ncdf/ (accessed on 15 May 2023).
60. Wickham, H.; Averick, M.; Bryan, J.; Chang, W.; McGowan, L.D.; François, R.; Grolemund, G.; Hayes, A.; Henry, L.; Hester, J.; et al. Welcome to the tidyverse. *J. Open Source Softw.* **2019**, *4*, 1686. [CrossRef]
61. Pebesma, E.; Bivand, R. *Spatial Data Science: With Applications in R*; CRC Press: Boca Raton, FL, USA, 2023.
62. Carslaw, D.C.; Ropkins, K. Openair—An R Package for Air Quality Data Analysis. *Environ. Model. Softw.* **2012**, *27*, 52–61. [CrossRef]
63. Schulzweida, U. CDO User Guide. Available online: https://code.mpimet.mpg.de/projects/cdo/embedded/index.html (accessed on 20 May 2023).
64. Xian, T.; Guo, J.; Zhao, R.; Su, T.; Li, Z. The Impact of Urbanization on Mesoscale Convective Systems in the Yangtze River Delta Region of China: Insights Gained from Observations and Modeling. *J. Geophys. Res. Atmos.* **2023**, *128*, e2022JD037709. [CrossRef]
65. Vo, T.T.; Hu, L.; Xue, L.; Li, Q.; Chen, S. Urban Effects on Local Cloud Patterns. *Proc. Natl. Acad. Sci. USA* **2023**, *120*, e2216765120. [CrossRef]
66. Xu, G.; Fu, S.; Liu, J.; Shang, R.; Luo, Y. A Satellite Observational Study of Topographical Effects on Daytime Shallow Convective Clouds. *Remote Sens.* **2023**, *15*, 5542. [CrossRef]
67. Craven, J.P.; Jewell, R.E.; Brooks, H.E. Comparison between Observed Convective Cloud-Base Heights and Lifting Condensation Level for Two Different Lifted Parcels. *Weather. Forecast.* **2002**, *17*, 885–890. [CrossRef]
68. Martucci, G.; Milroy, C.; O'Dowd, C.D. Detection of Cloud-Base Height Using Jenoptik CHM15K and Vaisala CL31 Ceilometers. *J. Atmos. Ocean. Technol.* **2010**, *27*, 305–318. [CrossRef]
69. Williams, A.P.; Schwartz, R.E.; Iacobellis, S.; Seager, R.; Cook, B.I.; Still, C.J.; Husak, G.; Michaelsen, J. Urbanization Causes Increased Cloud Base Height and Decreased Fog in Coastal Southern California. *Geophys. Res. Lett.* **2015**, *42*, 1527–1536. [CrossRef]
70. Wang, J.; Rossow, W.B.; Zhang, Y. Cloud Vertical Structure and Its Variations from a 20-Yr Global Rawinsonde Dataset. *J. Clim.* **2000**, *13*, 3041–3056. [CrossRef]
71. Free, M.; Sun, B.; Yoo, H.L. Comparison between Total Cloud Cover in Four Reanalysis Products and Cloud Measured by Visual Observations at U.S. Weather Stations. *J. Clim.* **2016**, *29*, 2015–2021. [CrossRef]